Energy transport systems for semiconductors: Analysis and simulation

Joseph W. Jerome[*] *and Chi-Wang Shu*[†]

Abstract. Moment models of carrier transport, derived from the Boltzmann equation, have made possible the simulation of certain key effects through such realistic global assumptions as energy dependent mobility functions. Some of these effects are not discerned via classical drift-diffusion models, which are primarily local in nature. In this paper, analysis and simulation of a recently developed energy transport model, the ET model, will be presented. This model, intermediate between the hydrodynamic and drift-diffusion models, was developed at the University of Illinois. The algorithms employed are the essentially non-oscillatory shock capturing algorithms, developed at UCLA during the last decade. Mathematical results will be presented as well, for the one dimensional steady state model. Informative comparisons with the hydrodynamic model will be presented. One carrier transport is studied.

1991 Mathematics Subject Classification: 35J65, 82A70, 65C20, 76N10, 35L65

1. Introduction

In this paper, an energy transport semiconductor device model, with steady state described by a nonlinear elliptic system, is introduced, analyzed and simulated, via numerical methods originally designed for conservation law systems. Energy transport (ET) systems have become topical in device modeling during the last decade, as an alternative to drift-diffusion systems, as it has become clear that global dependence of critical quantities, such as carrier mobilities, on energy and/or temperature, is essential if certain phenomena are to be modeled adequately. These include general carrier heating, velocity overshoot, and various small device features. Our development of the ET model follows that of [1] (see also [2]), which is based upon moments of the Boltzmann equation. These researchers attempted to utilize a microscopic relaxation time approximation, which would allow for nonparabolic energy bands

[*]The first author is supported by the National Science Foundation under grant DMS-9123208.

[†]The second author is supported by the Army Research Office under grant DAAL03-91-G-0123 and by the National Aeronautics and Space Administration under grant NAG1-1145. Computations were performed on the Cray YMP at the Pittsburgh Supercomputing Center.

and non-Maxwellian distribution functions. The approach also allows for parameter fitting of certain key quantities, via Monte-Carlo simulation of the Boltzmann equation. The ET model was developed, partly in response to the continuing debate concerning heat conduction processes in the hydrodynamic model. The absence of hyperbolic modes makes for essential mathematical simplification. The plan of the paper is as follows. In §2, we shall introduce the model, including a brief discussion of the physically motivating features. In the following §3, we shall outline an existence theory for the one dimensional, steady state model. The algorithm is described in §4, and simulation results, extending those of [4], are presented for two dimensional MESFET devices in §5; for illustrative purposes, comparisons are included with the corresponding hydrodynamic model. The latter contains hyperbolic modes related to the momentum subsystem, while the ET model does not possess such modes. In both cases, however, we employ a conservation law format, and numerical methods suitable for such systems. The ENO (essentially non-oscillatory) shock capturing method is our technique of choice.

2. The Steady State System

We shall consider steady state models, involving single carrier transport. The three dependent variables of the problem are electrostatic potential, ϕ, carrier concentration, n, and equivalent carrier temperature, T.

2.1. The System

The system is given as follows.

$$\begin{aligned} -\nabla\cdot(\epsilon\nabla\phi) + qn &= qn_d, && (2.1)\\ \nabla\cdot J &= 0, && (2.2)\\ \nabla\cdot S &= -\nabla\phi\cdot J - nC_{col}. && (2.3) \end{aligned}$$

Here, J and S represent the current density and energy density, respectively, and C_{col} is a collision rate. They are given by the expressions,

$$\begin{aligned} J &= q\{-\mu n\nabla\phi + \frac{k}{q}\nabla(\mu nT)\}, && (2.4)\\ S &= -Q(T)\{\frac{k^2}{q}\nabla(\mu nT^2) - \mu nkT\nabla\phi\}, && (2.5)\\ C_{col} &= c_1 q\{(1+\frac{1}{2}T)T - T_0\}, && (2.6) \end{aligned}$$

with the mobility μ and the effective flow factor $Q(T)$ functions of temperature; the latter function is assumed to preserve uniform ellipticity. Typical representations are:

$$\mu = \mu_0 T_0/T, \tag{2.7}$$

$$Q(T) = \frac{3}{2}(1 - \alpha kT/2). \tag{2.8}$$

Here, α is a fitting parameter. Also, μ_0 is a low field mobility constant, k is Boltzmann's constant, T_0 is the lattice temperature, c_1 is a numerical constant, q is a charge modulus constant, and ϵ is the dielectric constant. The function n_d is the nonnegative spatially dependent doping function. Boundary conditions are mixed Dirichlet/Neumann boundary conditions; on a one dimensional device, these are Dirichlet endpoint conditions.

2.2. Physical Motivation

The system (2.1), (2.2), and (2.3) is obtained by taking zeroth and second moments of the Boltzmann transport equation,

$$\frac{\partial f}{\partial t} + u \cdot \nabla_x f - \frac{q}{m} F \cdot \nabla_u f = C, \tag{2.9}$$

where f represents the electron probabilistic density, u the group velocity, F the electric field, and C the collision terms. The current density J and the energy flux S are defined by the moments,

$$J = -q \int u f_{odd}\, du, \quad S = \int \mathcal{E} u f_{odd}\, du, \tag{2.10}$$

where $\mathcal{E}$ denotes the (microscopic) carrier energy. The Boltzmann transport equation determines the relation of f_{even} to f_{odd}, and this relation is substituted into (2.10):

$$J = q[n\mu(E)F + \nabla(nD(E))], \tag{2.11}$$

$$S = -[n\mu^E(E)F + \nabla(nD^E(E))]. \tag{2.12}$$

Here, μ and μ^E are tensor moment expressions for the mobility coefficients, though in this paper isotropic assumptions lead to scalar expressions. The diffusion coefficients are determined by the Einstein relations. Finally, E denotes average energy/mass/volume: $E = \langle \mathcal{E} \rangle$.

Certain microscopic assumptions are incorporated; for precise formulations we refer the reader to the source paper [1]. The principal assumptions are:

1. Isotropic functions: $f_{even} = f_{even}(\mathcal{E})$;
2. Nonparabolic energy bands;
3. The temperature is a modified variable: $E = \frac{3}{2}kT(1 + \frac{5}{2}\alpha kT)$.

The mathematical system is a nonlinear parabolic system. When conservation variables, qn, nE/m are employed, the moment subsystem is a perturbed hyperbolic conservation system, with real eigenvalues for flux gradients, $f_i(u)_{x_i}$.

3. Existence Theory in One Dimension

We shall sketch the existence theory for the steady state ET model in one dimension. We find it helpful to introduce a new set of dependent variables.

3.1. Exponential Variables in One Dimension

In this subsection, we introduce a set of exponential variables. They will be used in the next subsection to deduce corresponding maximum principles. The latter facilitate the definition of an invariant map, whose fixed points coincide with the system solutions.

The exponential variables are similar to the quasi-Fermi levels of the drift-diffusion model. They are determined by implicit relations involving the variables ϕ, n, and nT; ϕ is the first variable of the new set. The variables v and z of the new set are implicitly given. Also, it is critical to interpret μ as an explicitly given (composite) function.

$$n(x) = \exp(c_0(\Phi(x) - v(x))), \tag{3.1}$$
$$n(x)T(x) = \exp(c_0(\Phi(x) - z(x))), \tag{3.2}$$

where

$$\Phi(x) = \int_a^x \mu(t)\phi'(t)\, dt. \tag{3.3}$$

We shall now rewrite the system in terms of these variables. Although μ must be explicit, the system is still strictly logically equivalent to the two systems defined in the previous section. We shall actually make use of the exponential variables when lagging has been employed in the original system as a means of defining the fixed point map.

$$-(d/dx)(\epsilon d\phi/dx) + q\exp([\Phi - v]c_0) = qn_d, \tag{3.4}$$
$$(d/dx)(\exp([\Phi - v]c_0)dv/dx) = 0, \tag{3.5}$$
$$(d/dx)(kQ(T)\exp([\Phi - z]c_0)dz/dx) = -d\phi/dx\ J - G(\Phi, v, z), \tag{3.6}$$

$$G(\Phi, v, z) = c_1 q\exp(c_0\Phi)\{(1 + \frac{1}{2}\exp([v - z]c_0))\exp(-zc_0) - T_0\exp(-vc_0)\}. \tag{3.7}$$

Note that in this system, $c_0 = \frac{q}{kT_0\mu_0}$, and that there is a simplified formula for the constant J: $J = -qv'n$, so that v' may be identified with carrier velocity. We shall agree to track right-left current flow, i. e. , $v' > 0$ and $J < 0$. The equation (3.5) is an example of Bernoulli's equation, with exponent 2, for v'. The solution is given by,

$$v'(x) = Y(x)\frac{1}{C - c_0\int_a^x Y(t)\, dt}, \tag{3.8}$$

where

$$Y(x) = \exp(-c_0\Phi(x)),\ \ C = \frac{1}{v'(a)} > 0. \tag{3.9}$$

We close this subsection with a relation for J.

Proposition 3.1. *The constant current J is negative and satisfies*

$$J = qe^{-c_0 v(x_*)} \frac{v(a) - v(b)}{b - a} / \int_a^b Y(x)\, dx, \tag{3.10}$$

for some $x_* \in (a, b)$.

Proof. Since J is constant, it may be evaluated at any x:

$$J = q \frac{e^{-c_0 v(x)}}{c_0 \int_a^x Y(t)\, dt - C}. \tag{3.11}$$

The appropriate value is $x = x_*$, where x_* is guaranteed, by the mean value theorem of integral calculus, applied to $\int_a^b v'(x)\, dx$, to satisfy

$$c_0 \int_a^{x_*} Y(x)\, dx - C = \frac{\int_a^b Y(x)\, dx}{v(a) - v(b)}. \tag{3.12}$$

The proposition follows from these relations.

3.2. Maximum Principles

The key to defining a fixed point map, $\mathcal{T}$, on the variables v and z is the establishment of maximum principles, which induce a mapping invariance property. In this section, we derive these necessary results. We begin by describing the map intuitively; ϕ is computed as a fractional step, if initial values of v and z are prescribed. This employs $\mu(v, z)$, as a means of determining Φ. System decoupling proceeds as follows. In (3.5), Φ and v are substituted in the exponential; in (3.6), Φ and v are substituted throughout, but z in $Q(T)$ only. New values, v^* and z^*, and hence the image coordinates of the map, are then computed via the decoupling.

If boundary values of v are chosen so that $v(a) < v(b)$, then the discussion of the previous subsection shows that $v' > 0$, hence v satisfies the elementary maximum principle,

$$v(a) \le v \le v(b). \tag{3.13}$$

A separate argument shows this to be the case if $v(a) = v(b)$. Prior to passing to a discussion of boundary values for z, we note that the specifications,

$$\phi(a) \le \phi(b), \;\; n(b) \le n(a), \tag{3.14}$$

imply $v(a) \le v(b)$, hence, (3.13). Bounds for z are considered next. The possible change of sign of ϕ' makes standard approaches inapplicable. We begin as follows.

Lemma 3.2. *Let $\gamma = \min(0, \gamma_*)$, where $\exp(c_0\gamma_* - c_0 v(a)) - \inf n_d = 0$. If Y is the function defined in (3.9), then $\psi = (Y^{-1} - \exp(c_0\gamma))^- \equiv 0$ if (3.14) holds, where $t^- = t - t^+$. In particular, $Y^{-1} \ge \exp(c_0\gamma)$ and Φ of (3.4) satisfies, without restriction on z,*

$$\Phi \ge \Phi_{min} := \gamma. \tag{3.15}$$

Proof. The assumption, (3.14), guarantees that $\psi(a) = \psi(b) = 0$. We shall employ ψ as a test function in the weak formulation of (3.4). Now one sees that the function,

$$qn - qn_d = q(\exp([\Phi - v]c_0) - n_d), \tag{3.16}$$

arising in (3.4), is nonpositive on the set, $\{\Phi \leq \gamma_*\}$. The integrated product of this function with ψ is therefore nonnegative. Moreover,

$$\int_a^b \epsilon\phi'\psi'\, dx = \int_{\{\Phi\leq\gamma\}} \frac{\epsilon Y}{\mu c_0} \mid \psi'(x) \mid^2 \, dx \geq 0,$$

so that, from the weak relation, the latter integral vanishes. We conclude that $\psi \equiv 0$, and the lemma follows.

Definition 3.3. We assume the existence of a root, $z = z_{**}$, satisfying

$$0 = c_1 q e^{c_0\Phi_{min}}[(1 + \frac{1}{2}e^{c_0(v(b)-z_{**})})e^{-c_0 z_{**}} - T_0 e^{-c_0 v(b)}] + \frac{q^2(v(b) - v(a))}{\epsilon Y_{min}} \frac{\sup n_d}{b-a} e^{-c_0 v(a)}, \tag{3.17}$$

where

$$Y_{min} = \exp(-c_0(\phi(b) - \phi(a))\mu_0 T_0 e^{z_{**}-v(a)}). \tag{3.18}$$

Moreover, we select the root, $z = z_*$, satisfying

$$0 = c_1 q e^{c_0\Phi_{min}}[(1 + \frac{1}{2}e^{c_0(v(a)-z_{*})})e^{-c_0 z_{*}} - T_0 e^{-c_0 v(a)}] - \frac{q^2(v(b) - v(a))}{\epsilon Y_{min}} \frac{\sup n_d}{b-a} e^{-c_0 v(a)}. \tag{3.19}$$

Finally, we define $z_{max} = \max(z(a), z(b), z_{**})$ and $z_{min} = \min(z(a), z(b), z_*)$.

Proposition 3.4. *Suppose that the solution ϕ of (3.4) satisfies*

$$\phi'(a) \geq 0, \;\; \phi'(b) \leq 0, \tag{3.20}$$

for $v(a) \leq v \leq v(b)$ and $z_{min} \leq z \leq z_{max}$. Then the bound,

$$\mid \phi' \mid \leq \frac{q(b-a)}{\epsilon} \sup n_d, \tag{3.21}$$

holds, and the function G of (3.7) satisfies

$$G(\Phi, v, z) + \phi' J \;\; \leq \;\; 0, \;\; z \geq z_{max}, \tag{3.22}$$

$$G(\Phi, v, z) + \phi' J \;\; \geq \;\; 0, \;\; z \leq z_{min}. \tag{3.23}$$

In particular, for solutions of (3.6), the maximum principle follows:

$$z_{min} \leq z \leq z_{max}. \tag{3.24}$$

Proof. The bound (3.21) follows directly from (3.4) and the hypotheses, (3.20). The relations (3.10) and (3.21), and the definition of G in (3.7), lead to (3.22) and (3.23). The maximum principle for (3.6) follows as in the proof of Lemma 3.2, via the respective choices of positive and negative parts for test functions, $(z - z_{max})^+$, $(z - z_{min})^-$, yielding upper and lower bounds.

3.3. The Fixed Point Map

We shall prove that a solution exists in this subsection.

Theorem 3.5. *Let $\mathcal{G} = (a, b)$, and suppose (3.17) and (3.20) hold. Set K equal to the closed convex subset of $\prod_1^2 L_2(\mathcal{G})$ defined by,*

$$K = \{[v, z] : v(a) \leq v \leq v(b), \;\; z_{min} \leq z \leq z_{max}\}. \tag{3.25}$$

Let $\mathcal{T}$ be the mapping, invariant on K, introduced in §3.2. Then $\mathcal{T}$ is well-defined, acts continuously on K, and has relatively compact range. In particular, $\mathcal{T}$ has a fixed point, $[v, z]$, and the triple, $[\phi(v, z), v, z]$, defines a solution of the steady state system, (2.1), (2.2), and (2.3).

Proof. The fact that $\mathcal{T}$ is well-defined follows from quadratic minimization applied to (3.5) and convex minimization applied to (3.6); note that G is decreasing in z. These are individual gradient equations. The details of a similar argument may be found in [3]. Here, a slight modification is required for the determination of ϕ, as computed in the fractional step. What is necessary is a preliminary mapping of $\phi \mapsto \Phi$. The relative compactness follows from H^1 bounds for v^* and z^*; test functions $v^* - v_{int}$ and $z^* - z_{int}$ are employed, where the linear interpolants of the boundary values are subtracted. The routine estimates here employ the maximum principles.

Continuity is established for v^* and z^* by using the components of the difference of two solutions as test functions: $v_2^* - v_1^*$, $z_2^* - z_1^*$. The preliminary continuity of the dependence of ϕ must first be established, however. We illustrate this. Starting with the identity,

$$\phi_2'' - \phi_1'' = \frac{q}{\epsilon}(\exp([\Phi_2 - v_2]/c_0) - \exp([\Phi_1 - v_1]/c_0)), \tag{3.26}$$

we employ $\psi = \phi_2 - \phi_1$ as test function. This yields, after some estimation, constants C_1 and C_2 such that

$$\|\psi'\|_{L_2}^2 \leq C_1\|\psi\|_{L_2}^2 + C_2\|\psi\|_{L_2}(\|\mu_2 - \mu_1\|_{L_2} + \|v_2 - v_1\|_{L_2}). \tag{3.27}$$

Here, we have used previously derived estimates for ϕ', as well as the maximum principles and elementary calculus. Though the positive function μ, in the definition of Φ, need not be continuous, it can be approximated by such, and thus the mean value theorem of integral calculus may be employed. The Poincare inequality in one dimension, applied to ψ, allows us to conclude continuous H^1 dependence of ϕ upon L_2 variation of v and z if $b - a$ is sufficiently small; in this case, the terms involving $\|\psi\|_{L_2}$, on the right hand side of (3.27), can be absorbed on the left hand side. However, a simple change of variable then gives the general result. The arguments for the continuity of the other variables follow closely in spirit Lemmas 3.3 and 3.4 of [3]. An application of the Schauder fixed point theorem then yields a fixed point. This can be identified with either set of dependent variables.

Remark. The condition (3.20) appears to hold approximately, on the basis of numerical simulations, carried out on $n^+ - n - n^+$ diodes. A so-called neutral region surrounds the contacts, and the field is approximately zero.

4. Numerical Algorithm

We shall only briefly describe the algorithm used in this paper, namely the ENO scheme developed in [7] and [8]. The ENO scheme is designed for a system of hyperbolic conservation laws of the form,

$$u_t + \sum_1^d f_i(u)_{x_i} = g(u, x, t), \tag{4.1}$$

where $u = (u_1, \cdots, u_m)^T$, $x = (x_1, \cdots, x_m)$, and the hyperbolicity condition,

$$\sum_1^d \xi_i \frac{\partial f_i}{\partial u} \text{ is diagonalizable, with real eigenvalues,}$$

holds for any real $\xi = (\xi_1, \cdots, \xi_d)$. An initial condition is adjoined to (4.1).

For systems of conservation laws, local field by field decomposition is used, to resolve waves in different characteristic directions. For this purpose, analytical expressions are needed for the eigenvalues and eigenvectors of the Jacobian matrix, which are readily available for the current ET system. Multidimensional regions are treated dimension by dimension: when computing $f_i(u)_{x_i}$ in any particular direction, variables in all other directions are kept constant, and the Jacobians are treated in this direction. This, in essence, reduces the determination of the scheme to the case of a single conservation law in one spatial dimension. Thus, to describe the schemes, consider the scalar one dimensional problem, and a conservative approximation of the spatial operator given by

$$L(u)_j = -\frac{1}{\triangle x}(\hat{f}_{j+\frac{1}{2}} - \hat{f}_{j-\frac{1}{2}}). \tag{4.2}$$

Here, the numerical flux $\hat{f}$ is assumed consistent:

$$\hat{f}_{j+\frac{1}{2}} = \hat{f}(u_{j-l}, \cdots, u_{j+k}); \qquad \hat{f}(u, \cdots, u) = f(u). \tag{4.3}$$

The conservative scheme (4.2), which characterizes the $\hat{f}$ divided difference as an approximation to $f(u)_x$, suggests that $\hat{f}$ can be identified with an appropriate function h satisfying

$$f(u(x)) = \int_{x-\frac{\triangle x}{2}}^{x+\frac{\triangle x}{2}} h(\xi)\, d\xi. \tag{4.4}$$

If H is any primitive of h, then h can be computed from H'. H itself can be approximated by polynomial interpolations using Newton's divided difference method, beginning with differences of order one, since the constant term is arbitrary. The necessary divided differences of H, of a given order, are expressed as constant multiples of those of f of order one lower. After the polynomial Q of degree $r+1$ has been constructed, set

$$\hat{f}_{j+\frac{1}{2}} = \frac{d}{dx} Q(x)_{|_{x=x_{j+\frac{1}{2}}}}, \tag{4.5}$$

to obtain an rth order method. The main ingradient of the ENO method is the adaptive choice of stencil: it begins with a starting point to the left or right of the current "cell" by means of upwinding, as determined by the sign of the derivative of a selected flux (or the eigenvalue of the Jacobian in the system case); as the order of the divided differences is increased, the divided differences themselves determine the stencil: the "smaller" divided difference is chosen from two possible choices at each stage, ensuring a smoothest fit.

Steady states are reached by explicit time stepping using nonlinearly stable (total-variation-diminishing) Runge-Kutta methods [7]. Special attention is paid to achieve efficient vectorization for computations on Cray supercomputers. For details of the efficient implementation, see [6].

5. Simulations

We now present numerical simulation results for a one carrier, two dimensional MESFET device using the ET model. A similar device was simulated earlier by us using the HD model and the same ENO algorithm in [4]. The third order ENO shock-capturing algorithm, as described briefly in Section 4 and in more detail in [8], is applied to the hyperbolic part (the first derivative part) of the two dimensional ET system. A nonlinearly stable third order Runge-Kutta time discretization [7] is used for the time evolution towards steady states. The forcing terms (the derivative-free part) are treated in a time consistent way in the Runge-Kutta time stepping. The double derivative terms are approximated by standard central differences owing to their dissipative nature. The coupled Poisson equation (2.1) is solved by Successive Over-Relaxation (SOR) or the Conjugate Gradient (CG) method. Initial conditions are chosen as $n = n_d$ for the concentration and $T = T_0$ for the temperature. A continuation method is used to reach the steady state: the voltage bias is taken initially as zero and is gradually increased to the required value, with the steady state solution of a lower biased case used as the initial condition for a higher one.

The two dimensional MESFET we simulate is of the size $0.9 \times 0.2\mu m^2$. The source and the drain occupy $0.1\mu m$ and $0.2\mu m$ at the upper left and the upper right, respectively, with the gate occupying $0.2\mu m$ at the upper middle (Figure 1, left. Here and in what follows, the units shown in the graphs for n or n_d are $10^{12}cm^{-3}$). The doping is defined by $n_d = 3 \times 10^{17}cm^{-3}$ in $[0, 0.1] \times [0.15, 0.2]$ and in $[0.7, 0.9] \times [0.15, 0.2]$, and $n_d = 1 \times 10^{17}cm^{-3}$ elsewhere, with abrupt junctions (Figure 1, right). A uniform grid of 144×32 points is used. Notice that even if we may not have shocks in the solution, the final steady state solution has a sharp transition around the junction. With the relatively coarse grid we use, the non-oscillatory shock capturing feature of the ENO algorithm is essential for the stability of the

numerical procedure.

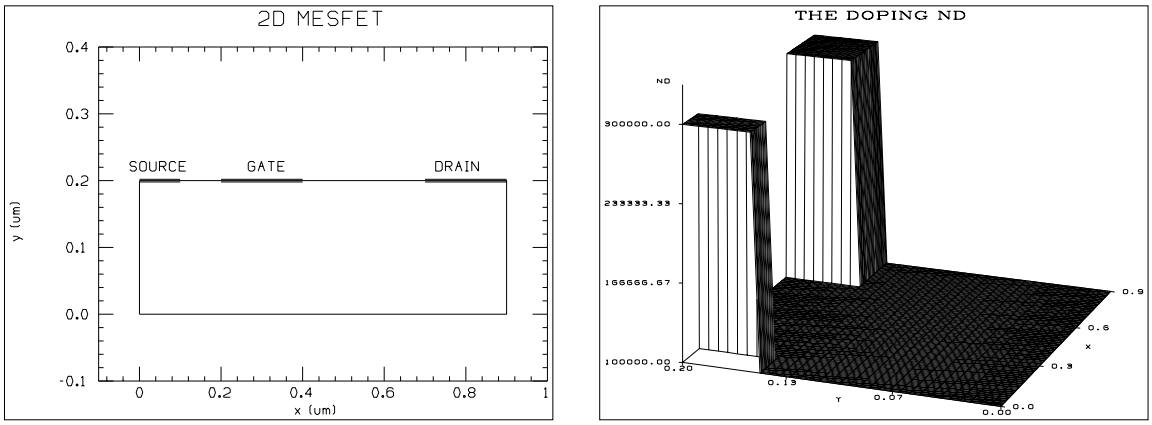

Figure 1: Two dimensional MESFET. Left: the geometry; Right: the doping n_d

We apply, at the source and drain, a voltage bias $vbias = 2V$. The gate is a Schottky contact, with a negative voltage bias $vgate = -0.8V$ and a very low concentration value $n = 3.9 \times 10^5 cm^{-3}$ obtained from Equation (5.1-19) of [5]. The lattice temperature is taken as $T_0 = 300°K$. The numerical boundary conditions are summarized as follows (where $\Phi_0 = \frac{k_b T}{q} \ln\left(\frac{n_d}{n_i}\right)$ with $k_b = 0.138 \times 10^{-4}$, $q = 0.1602$, and $n_i = 1.4 \times 10^{10} cm^{-3}$ in our units):

- At the source ($0 \le x \le 0.1, y = 0.2$): $\Phi = \Phi_0$ for the potential; $n = 3 \times 10^{17} cm^{-3}$ for the concentration and $T = 300°K$ for the temperature.
- At the drain ($0.7 \le x \le 0.9, y = 0.2$): $\Phi = \Phi_0 + vbias = \Phi_0 + 2$ for the potential; $n = 3 \times 10^{17} cm^{-3}$ for the concentration and $T = 300°K$ for the temperature.
- At the gate ($0.2 \le x \le 0.4, y = 0.2$): $\Phi = \Phi_0 + vgate = \Phi_0 - 0.8$ for the potential; $n = 3.9 \times 10^5 cm^{-3}$ for the concentration and $T = 300°K$ for the temperature.
- At all other parts of the boundary ($0.1 \le x \le 0.2, y = 0.2$; $0.4 \le x \le 0.7, y = 0.2$; $x = 0, 0 \le y \le 0.2$; $x = 0.9, 0 \le y \le 0.2$; and $0 \le x \le 0.9, y = 0$), all variables are equipped with Neumann boundary conditions.

Notice that the boundary conditions for the concentration n and the temperature T are the same as those used in [4] for the HD model, although in the HD model one also has to specify boundary conditions for velocities. These boundary conditions may not be adequate, as is evident from some serious boundary layers observable in Figures 2 through 4. ENO methods, owing to their upwind nature, are robust to different boundary conditions (including over-specified boundary conditions in hydrodynamic models), and do not exhibit numerical difficulties in the presence of

such boundary layers, even with the extremely low concentration prescribed at the gate (approximately 10^{-12} relative to the high doping).

In Figures 2 through 4, we show pictures of the concentration n, temperature T, and the potential Φ. Surfaces of the ET solution are shown at the left, and cuts at $y = 0.175$, which cut through the middle of the high doping "blobs" horizontally, are shown at the right. For those cuts we show both the ET ("+" symbols) and HD (solid line) simulation results in order to see a comparison.

Notice that ET and HD results agree reasonably well for the concentration n and for the potential Φ, but not so well for the temperature T. Whether this shows any essential difference of the two models, or is simply due to some inadequacy in the choice of the various empirical parameters in the ET model, is not clear, and is currently under additional investigation.

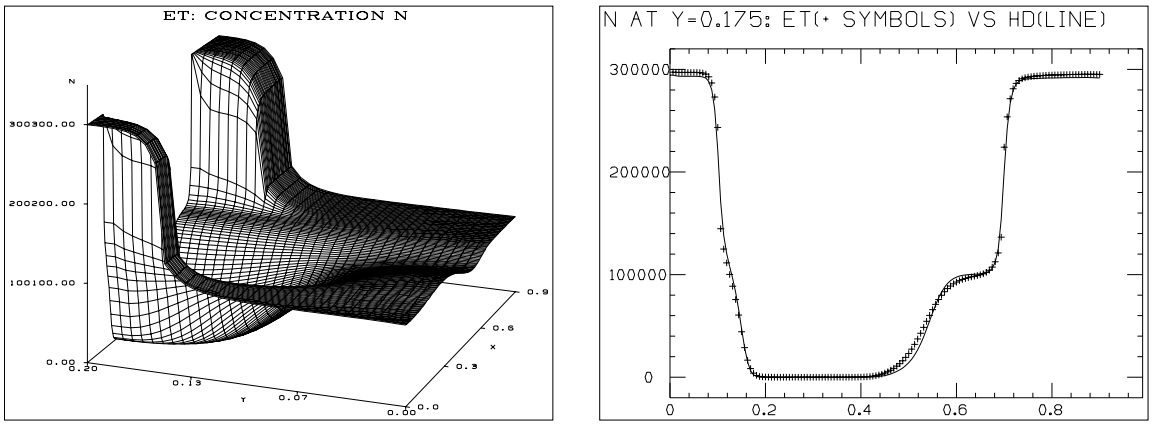

Figure 2: Two dimensional MESFET, concentration n. Left: surface of the ET solution; Right: cut at $y = 0.175$ (ET—"+" symbols; HD—line)

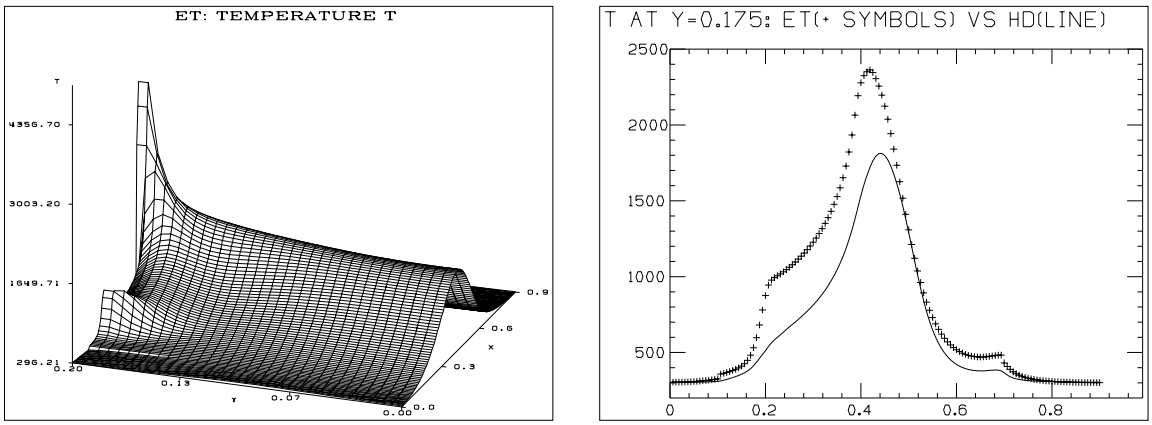

Figure 3: Two dimensional MESFET, temperature T. Left: surface of the ET solution; Right: cut at $y = 0.175$ (ET—"+" symbols; HD—line)

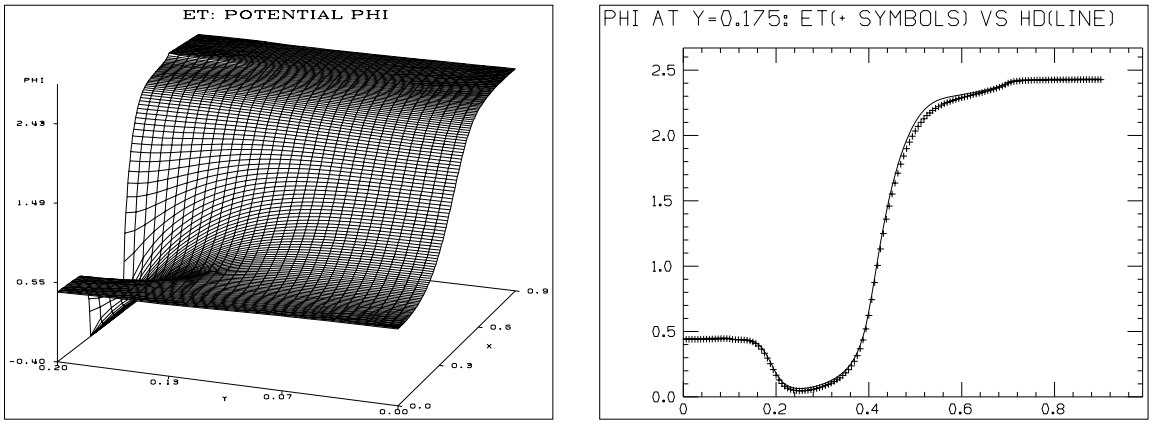

Figure 4: Two dimensional MESFET, potential Φ. Left: surface of the ET solution; Right: cut at $y = 0.175$ (ET—"+" symbols; HD—line)

References

[1] Chen, D., E. Kan, U. Ravaioli, K. Hess, and R. Dutton. Steady-state macroscopic transport equations and coefficients for submicron device modeling. IEEE Transactions Electron Devices, to appear.

[2] Chen, D., E. Kan, U. Ravaioli, C.-W. Shu, and R. Dutton. An improved energy transport model including nonparabolicity and non-Maxwellian distribution effects. IEEE Electron Device Letters 13:1 (1992), 26–28.

[3] Jerome, Joseph W., Consistency of semiconductor modelling: An existence/stability analysis for the stationary van Roosbroeck system.SIAM J. Appl. Math. 45:4 (1985), 565–590.

[4] Jerome, Joseph W., and Chi-Wang Shu. Energy models for one-carrier transport in semiconductor devices. Proceedings, IMA Workshop on Semiconductors. Springer-Verlag, 1993.

[5] Selberherr, S., Analysis and Simulation of Semiconductor Devices. Springer-Verlag, Wien-New York, 1984.

[6] Shu, C.-W., G. Erlebacher, T. Zang, D. Whitaker, and S. Osher. High-order ENO schemes applied to two- and three-dimensional compressible flow. Applied Numer. Math. 9 (1992), 45–71.

[7] Shu, C.-W., and S.J. Osher. Efficient implementation of essentially non-oscillatory shock capturing algorithms. J. Comp. Phys. 77 (1988), 439–471.

[8] Shu, C.-W., and S.J. Osher. Efficient implementation of essentially non-oscillatory shock capturing schemes, II. J. Comp. Phys. 83 (1989), 32–78.